Inorganica Chimica Acta 421 (2014) 246–254

Contents lists available at ScienceDirect

Inorganica Chimica Acta

journal homepage: www.elsevier.com/locate/ica

$\{[Co_2(btec)(2,2'\text{-bipy})_2]\cdot H_2O\}_n$ metal–organic framework: Structure and activity in the solvent-free oxidation of cyclohexene with oxygen

Jianmin Hao *, Sijia Li, Limin Han, Lin Cheng, Quanling Suo, Yang Xiao, Xiaoli Jiao, Xuemin Feng, Weiwei Bai, Xiaofei Song

Chemical Engineering College, Inner Mongolia University of Technology, Hohhot 010051, PR China

ARTICLE INFO

Article history:
Received 26 February 2014
Received in revised form 11 May 2014
Accepted 10 June 2014
Available online 18 June 2014

Keywords:
Metal–organic framework
Cobalt
Heterogeneous catalysis
Cyclohexene oxidation
Oxygen

ABSTRACT

A Co (II) metal–organic framework (MOF) $\{[Co_2(btec)(2,2'\text{-bipy})_2]\cdot H_2O\}_n$ (H_4btec: 1,2,4,5-benzenetetracarboxylic acid; 2,2′-bipy: 2,2′-bipyridine) was hydrothermally synthesized and characterized using X-ray crystallographic analysis, Fourier transform infrared spectroscopy, elemental analysis, X-ray diffraction, scanning electron microscopy, transmission electron microscopy and N_2 adsorption/desorption. Its catalytic performance was examined for the allylic oxidation of cyclohexene with oxygen under solvent-free conditions. It acted as a heterogeneous catalyst, which was deactivated in catalyst recycling and regenerated through treatment with a $scCO_2$-expanded ethanol system. The inhibitive effect of H_4btec and other ligands on cyclohexene oxidation was detected, presumed to be caused by hydrogen-bonding interaction between the H_4btec and a 2-cyclohexene-1-hydroperoxide intermediate.

Introduction

The selective oxidation of cyclohexene is an essential chemical process for the current chemical industry because its products, such as alcohols, ketones, epoxides, and acids, are chemical intermediates used for synthesizing polymers, drugs, agrochemicals, and surfactants [1]. Both the C=C double bond and the allylic C–H bond in cyclohexene are in active positions, which are prone to oxygenation for forming a great variety of products [2]. Because of increased environmental concerns, solvent-free benign oxidations that use heterogeneous catalyst and clean oxidants are favored [3]. Notably, product distribution depends on the catalysts and oxidants used [4,5]. As an oxidant, molecular oxygen has attracted much more attention because it is inexpensive, readily available, and environmentally benign compared with other oxidants [6,7]. Recently, certain heterogeneous catalysts, including metal-containing redox molecular sieves or metal complexes, oxides, and nanoparticles were researched in the oxidation of cyclohexene. For example, CrMCM-41 was discovered to be an efficient catalyst for the oxidation of cyclohexene, in which the conversion was 52.2% and the total selectivity of 2-cyclohexene-1-ol (Cy-ol), 2-cyclohexene-1-one (Cy-one), and 2-cyclohexene-1-hydroperoxide (Cy-HP) was 96.6% in the conditions of 1 atm O_2 and 343 K [8]. Chitosan-supported salophen Mn (III) complexes exhibited high catalytic activity in cyclohexene oxidation with a turnover number of 11.3×10^4, selectivity of 93.3% for Cy-ol, Cy-one, and Cy-HP at 343 K and ambient oxygen pressure [9].

The design and synthesis of metal–organic frameworks is increasingly crucial because of their special physical properties and potential applications in electronic, magnetic, optical, absorbent, and catalytic materials [10–13]. In the field of crystal engineering, the versatility of molecular chemistry enables the production of a great variety of polytopic organic ligands with different functionalities [14]. One ligand, H_4btec, is well known for having four rigid and symmetrical carboxyl groups that can construct stable, porous, and multidimensional frameworks through various coordination modes through the complete or partial deprotonation of carboxyl groups [15–17]. The stability of metal–organic frameworks containing H_4btec and other ligands can be enhanced by forming hydrogen bonds because H_4btec can act as a hydrogen-bond acceptor or hydrogen-bond donor. MOFs are promising materials for application in catalysis because they possess single-site active species characteristic of homogeneous catalysts, combined with the advantages of easy separation and recycling typical of heterogeneous catalysts. A new extended metal–organic framework $[Cu(H_2betc)(bipy)]_\infty$ (bipy = 2,2′-bipyridine) for cyclohexene oxidation was hydrothermally synthesized by Brown et al., which presented a high conversion of 64.5% and selectivity of 73.1% for cyclohexene epoxide [18]. The copper metal–organic framework

* Corresponding author. Tel./fax: +86 471 6575675.
E-mail address: haojmin@gmail.com (J. Hao).

http://dx.doi.org/10.1016/j.ica.2014.06.005
0020-1693/

[Cu(bpy)(H_2O)$_2$(BF_4)$_2$(bpy)] (bpy = 4,4′-bipyridine) exhibited promising catalytic activity and a high selectivity of 90% for Cy-HP in the allylic oxidation of cyclohexene with molecular oxygen as the only oxidant in the absence of solvent [19].

In this study, a Co (II) metal–organic framework {[Co_2(btec)(2, 2′-bipy)$_2$]·H_2O}$_n$ was synthesized using a hydrothermal method in accordance with the literature [20–22]. Its composition and structure was characterized and its catalytic activity in the selective oxidation of cyclohexene with molecular oxygen under solvent-free conditions was discussed in detail.

2. Experimental

2.1. Catalysts preparation and regeneration

{[Co_2(btec)(2,2′-bipy)$_2$]·H_2O}$_n$ was prepared under hydrothermal conditions. All the reagents were purchased commercially and used as delivered. In a typical synthesis, the reaction mixture of $Co(NO_3)_2{\cdot}6H_2O$ ($\geqslant$99%, 0.291 g), H_4btec (98%, 0.254 g), 2,2′-bipyridine (AR, 0.156 g) and redistilled water (15 mL) in a molar ratio of 1:1:1:833 was loaded in a 25-mL Teflon-lined stainless steel autoclave and the pH was adjusted to 8–9 by using $NH_3{\cdot}H_2O$. The autoclave was heated at 433 K for 120 h and slowly cooled to room temperature at 2.5 K/h. The product was filtered, washed with distilled water, and air-dried at room temperature. The product was in the form of wine block crystals with average quality of 0.2883 g per autoclave (yield: 82.6% based on Co). The product that was crushed was named Co-MOF-A and the product that was crushed, washed with ethanol (99%), and air-dried was named Co-MOF-B.

The amount of Co-MOF-B catalyst samples used after a catalytic cyclohexene oxidation run was collected. The used catalyst samples and 5 mL of ethanol were added to a 50-mL stainless steel batch reactor. After the reactor was heated to 308 K for 0.5 h, CO_2 was introduced into the reactor to 8 MPa, using a high-pressure liquid pump. The mixture was stirred continuously, using a Teflon-coated magnetic stir bar for 24 h. Subsequently, the reactor was cooled to room temperature and depressurized. The solid product was filtered and then dried at room temperature.

2.2. Catalysts characterization

The structural measurements of a single 0.12 × 0.1 × 0.08-mm wine crystal of the compound was performed using X-ray diffraction on a Bruker SMART 1000 CCD diffractometer with Mo Kα radiation (λ = 0.71073) at 296 K in the range of 2.69 < θ < 24.98. The structures were solved using direct methods and refined by implementing the full-matrix least-squares method on F^2 using the SHELX-97 crystallographic software package [23,24]. The crystallographic details of the structure of {[Co_2(btec)(2,2′-bipy)$_2$]·H_2O}$_n$ are summarized in Table S1 and the selected bond lengths and angles are given in Table S2. Fourier transform infrared (FTIR) spectra were recorded on a Nicolet FTIR spectrometer, using pellets of the materials diluted with KBr in the range of 4000–400 cm^{-1}. The Co content in the catalyst samples was determined by conducting inductively coupled plasma optical emission spectroscopy (ICP-OES) using a PerkinElmer Optima 7000 DV. Elemental analyses (C, H, and N) were performed using an Elementar VarioEL III elemental analyzer. Structural studies of the catalysts were performed using X-ray diffraction (XRD) on a Bruker-AXS D8 ADVANCE with Cu Kα in the 2θ range of 10–30°. A scanning electron microscope (SEM; Hitachi S-3400 N) was used to observe the surface morphology of the catalyst samples. Transmission electron microscopy (TEM) images were obtained using a FEI Tecnai G2 F20. The N_2 adsorption–desorption isotherms at 77 K were obtained using Micromeritics a ASAP 2020 instrument after an in situ automatic degassing procedure at 473 K. The density functional theory (DFT) calculations for Cy-HP and H_4btec interaction were performed using the GAUSSIAN 03 suite of programs. Since the Hybrid methods (one type of the density functional methods), such as B3LYP, tend to be the most commonly used methods, the proposed geometries of the hydrogen bonds between Cy-HP and H_4btec were optimized at the gas phase using B3LYP functional and the standard 6-31G(d) basis set.

2.3. Cyclohexene oxidation

Cyclohexene (Aladdin CP) and high-purity oxygen (99.999%) were used as-delivered. In typical reactions, a certain amount of substrate and catalyst were charged into a 50-mL stainless steel autoclave with a Teflon inner liner at room temperature. The reactor was heated to the desired temperature in an oil bath and a quantity of O_2 gas was then introduced into the reactor. The reaction runs were conducted whiles simultaneously stirring, using a magnetic stirrer. At the end of the reaction, the autoclave was cooled to room temperature and then depressurized. The catalyst was filtered and the product solution was diluted with ethanol. The main oxidation products, Cy-ol and Cy-one were identified by comparing with standard samples (retention time in GC), Cy-HP was analyzed using triphenylphosphine reduction because it is difficult to analyze by using GC [19]. The qualitative analysis of other by-products was examined using GC–MS. The composition of the reaction mixture was analyzed using a gas chromatograph (Shimadzu GC-14C, column RTX-50). The conversion was calculated as the moles of products formed (cyclohexene and the major product in a mole ratio of 1:1) divided by the initial moles of cyclohexene, and selectivity was calculated as the moles of a certain product divided by the total moles of products formed. Safety warning: Using compressed O_2 in the presence of organic substrates requires appropriate safety precautions and must be carried out in suitable equipment.

3. Results and discussion

3.1. Catalysts characterization

X-ray crystallographic analysis revealed that {[Co_2(btec)(2,2′-bipy)$_2$]·H_2O}$_n$ was crystallized in the orthorhombic space group C222(1). Fig. 1(a) shows that the Co (II) center displays a distorted octahedral geometry arrangement coordinating to two nitrogen atoms of one 2,2′-bipy ligand, three oxygen atoms of two different carboxylate groups, and one oxygen atom of a water molecule. Fig. 1(b) exhibits an infinite 2D lamellar structure. The four carboxylate groups of H_4btec present two types of coordination mode with the Co atoms: Two carboxylate groups on the same side offer four O atoms to form two bidentate chelating structures, and two carboxylate groups on the other side each offer one O atom to form two mono-dentate bridging structures. The bridging action of H_4-btec resulted in the formation of zig–zag chains running along the *a* axis, as shown in Fig. 1(c). The coordinated H_2O molecule acted as a bridge connecting two Co atoms, which resulted in the repeated emergence of symmetrical units along the *c* axis, as shown in Fig. 1(d).

The FT-IR spectra of H_4btec, Co-MOF-A, and Co-MOF-B are presented in Fig. 2. The H_4btec revealed one ν (CO) bond at 2017 cm^{-1} and distinct ν (O–H) bonds between 3540 and 2520 cm^{-1}, which were also visible in Co-MOF-A but invisible in Co-MOF-B. This indicated that an amount of unreacted H_4btec was mixed in Co-MOF-A. This result was further confirmed when the filtered solution obtained after washing Co-MOF-A with ethanol was analyzed

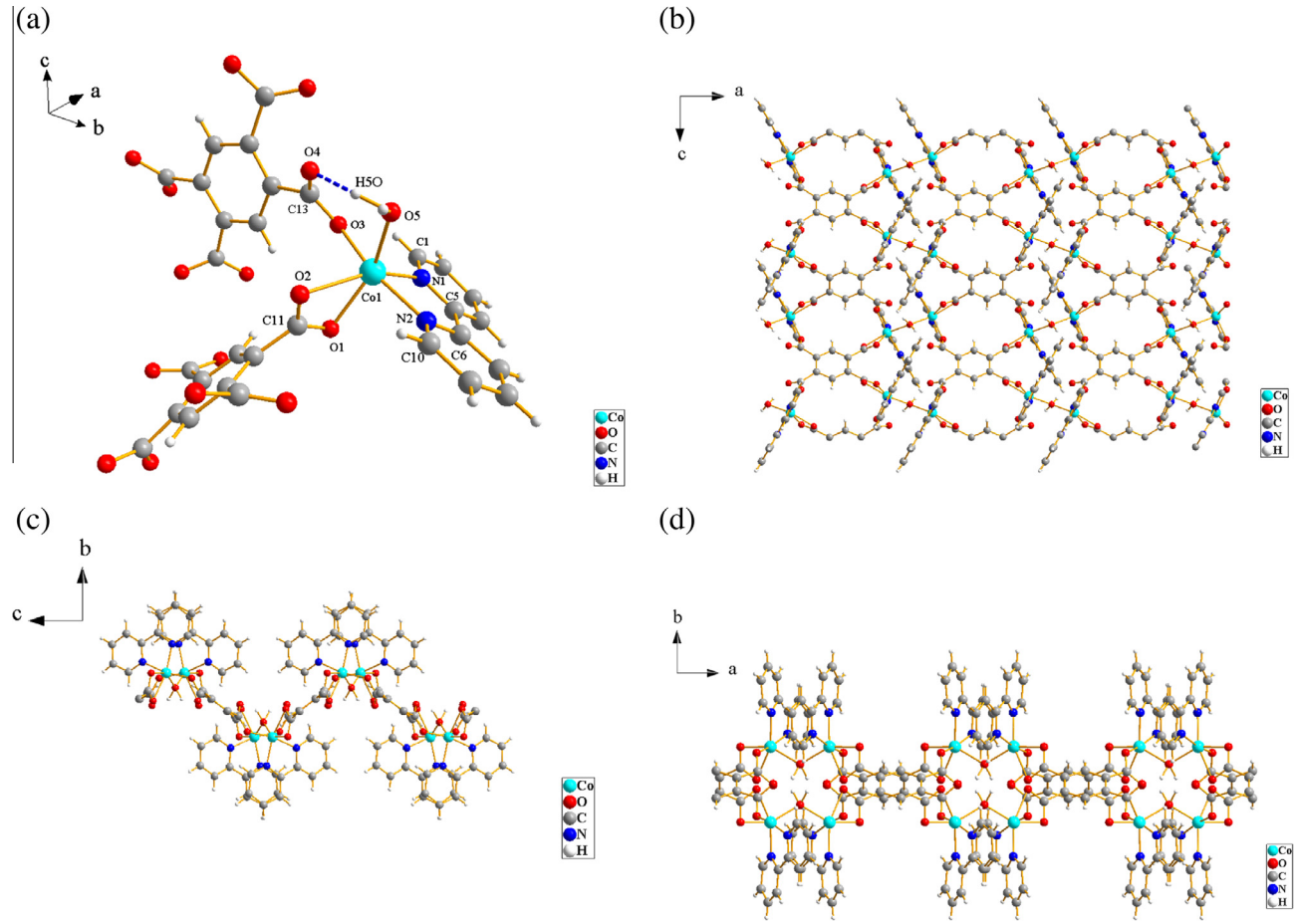

Fig. 1. A ball and stick representation of $\{[Co_2(btec)(2,2'\text{-bipy})_2]\cdot H_2O\}_n$ structure: (a) The local coordination environment of the compound. The intra-chain hydrogen bonding interaction is shown in broken lines; (b) The network of the compound along the *b* axis; (c) The network of the compound along the *a* axis; (d) The network of the compound along the c axis.

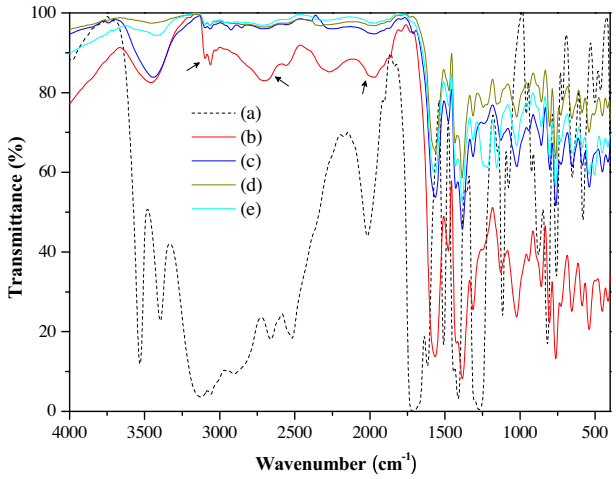

Fig. 2. FT-IR spectra of (a) H_4btec, (b) fresh Co-MOF-A catalyst, (c) fresh Co-MOF-B catalyst, (d) Co-MOF-B catalyst after one cyclohexene oxidation run and (e) Co-MOF-B catalyst after the fifth cyclohexene oxidation run.

using LC–MS (Shimadzu LCMS-2020) as shown in Fig. S1. The IR spectra of the fresh Co-MOF-B catalyst, Co-MOF-B catalyst after one cyclohexene oxidation run, and Co-MOF-B catalyst after the fifth cyclohexene oxidation run were the same.

Regarding the chemical composition of the catalyst samples in Table 1, the error of actual C, H, and N content was <±0.4% for

Table 1
Chemical composition of the catalyst samples.

Entry	Catalyst	Co (%)	C (%)	H (%)	N (%)
1	calculated	16.88	51.60	2.89	8.02
2	Co-MOF-A	15.16	51.21	2.84	8.21
3	Co-MOF-B	15.37	51.25	3.00	8.19
4[a]	Co-MOF-B	13.63	48.40	2.78	7.32
5[b]	Co-MOF-B	12.18	44.30	2.76	6.07

[a] After one cyclohexene oxidation run
[b] After the fifth cyclohexene oxidation run.

the fresh Co-MOF-A and Co-MOF-B catalyst samples. The Co, C, N and H contents in Co-MOF-B after catalytic reactions diminished simultaneously, which suggested that the O content increased. So it was suggested that certain oxidative organic residue were produced and adsorbed on the surface of MOF catalyst during the catalytic oxidation reactions. Compared with C, N and H contents, the Co content in Co-MOF-B catalyst after the reactions decreased in large proportion, which proved that Co leaching might occur during the reactions. However, this evidence was not reliable as a quantitative analysis of the Co leaching amount for the Co-MOF-B catalyst.

(Fig. 3) shows the XRD patterns of Co-MOF-A and Co-MOF-B catalyst samples. The fresh Co-MOF-A catalyst and fresh Co-MOF-B catalyst exhibit the same characteristic diffraction peaks, which illustrates that the residual H_4btec did not affect the crystalline structure. When the residual H_4btec was removed by washing with ethanol, the diffraction peaks of the fresh Co-MOF-B catalyst

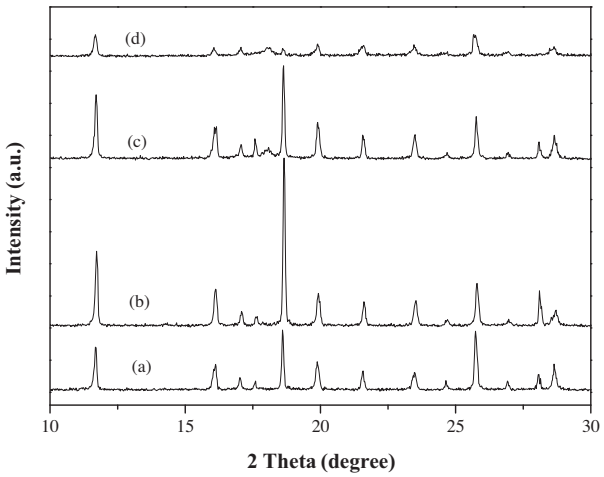

Fig. 3. XRD patterns of catalyst samples: (a) fresh Co-MOF-A catalyst; (b) fresh Co-MOF-B catalyst; (c) Co-MOF-B catalyst after one cyclohexne oxidation run; (d) Co-MOF-B catalyst after the fifth cyclohexene oxidation run.

intensified, suggesting that the inherent crystallinity of the catalyst is excellent. After cyclohexene oxidation, the characteristic diffraction peaks of Co-MOF-B were retained, but the intensity dropped and the reflection peaks broadened. This indicated that the crystalline structure of the catalyst was preserved during the reactions, but that the exterior surface was either covered by an amorphous substance or partially destroyed, which was revealed by the SEM images.

Using SEM provided some intuitive information regarding the surface properties of the Co-MOF-B catalyst during the catalytic reaction process. Small and irregularly shaped particles were formed and the surface of the particles was smooth and intact, as shown in Fig. 4(a) and (b). Comparing the results in Fig. 4(a) and (c), crystals damage was observed on the surface of the catalyst after one cyclohexene oxidation run. It was suggested that Co^{2+} leaching from the catalyst during the reaction lead to the partial collapse of the framework. During continuous stirring, partial collapsed framework agglutination occurred to form a filamentous organic residue coating on the surface of some catalyst particles during the catalyst recycling tests, as shown in Fig. 4(d), which is consistent with the results of the elemental analysis. The organic residue was physically adsorbed on the surface of the catalyst because the IR vibration frequency of the catalyst did not shift after the oxidation reaction.

The TEM images of the Co-MOF-B catalyst samples are presented in Fig. 5, which shows a layered 2D microstructure composed of nanoflakes. The nanoflakes were compact and did not exhibit a porous structure. Furthermore, the nanoflakes became smaller after one cyclohexene oxidation run because the crystal particles were crushed during the stirring process. The microstructure of the Co-MOF-B catalyst was mainly determined by the coordination structure and the crystal growth characteristics. The Co-MOF-B crystals exhibited a 2D (6, 4)-network because the chains were connected by coordinated H_2O molecule, and the adjacent 2D layers construct a 3D framework through π–π interactions between the aromatic groups of the 2,2'-bipy ligands [21].

3.2. Catalytic performances in cyclohexene oxidation

In the oxidation of cyclohexene, Cy-ol, Cy-one, and intermediate Cy-HP were produced along with several by-products such as cyclohexene oxide, 1,2-cyclohexanediol, hexanediol, adipic acid, and cyclohexanone, among others, as shown in Scheme 1. The potential reaction pathways in the catalytic oxidation of

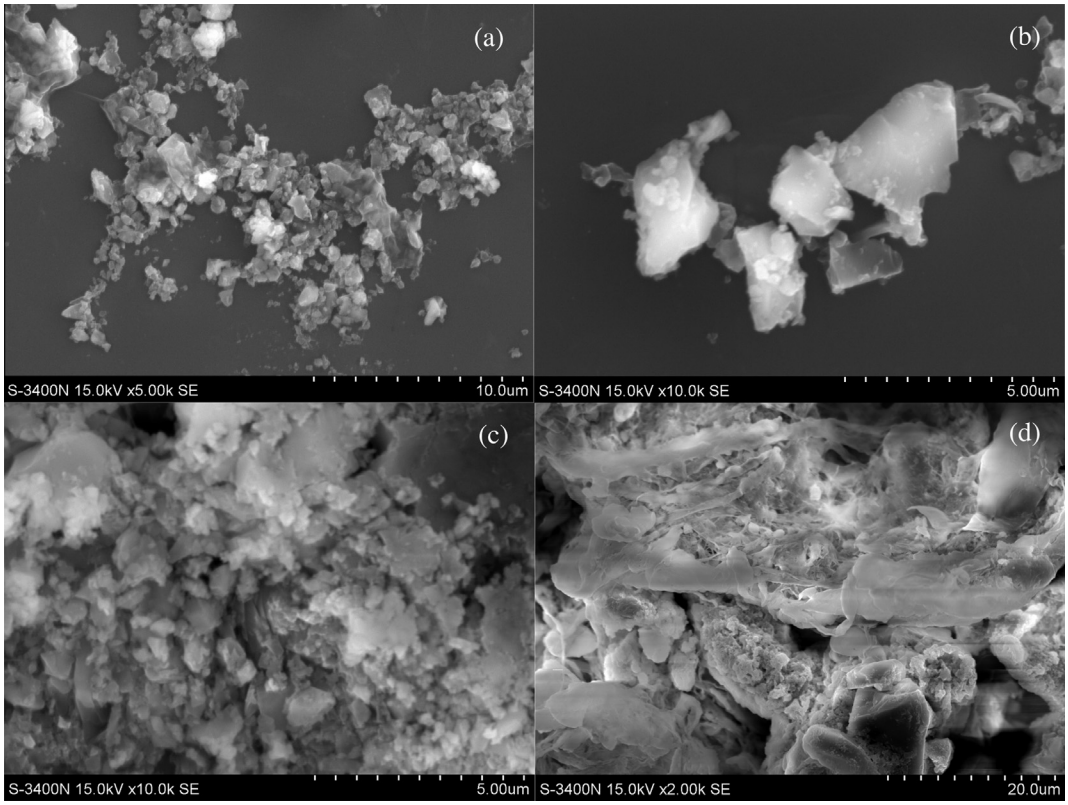

Fig. 4. SEM images of Co-MOF-B catalyst samples: (a) and (b) fresh catalyst; (c) catalyst after one cyclohexene oxidation run; (d) catalyst after the fifth cyclohexene oxidation run.

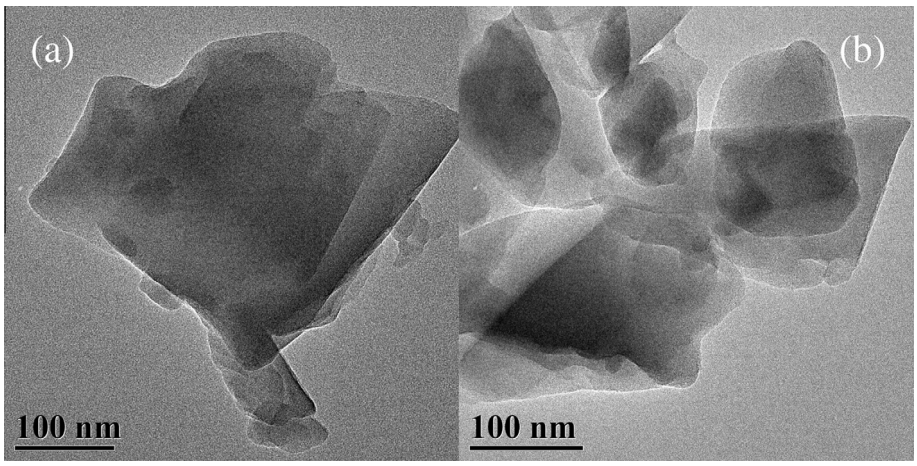

Fig. 5. TEM images of Co-MOF-B catalyst samples: (a) fresh catalyst; (b) catalyst after one cyclohexene oxidation run.

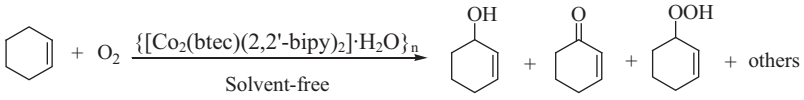

Scheme 1. Cyclohexene oxidation over $\{[Co_2(btec)(2,2'\text{-bipy})_2]\cdot H_2O\}_n$ catalyst.

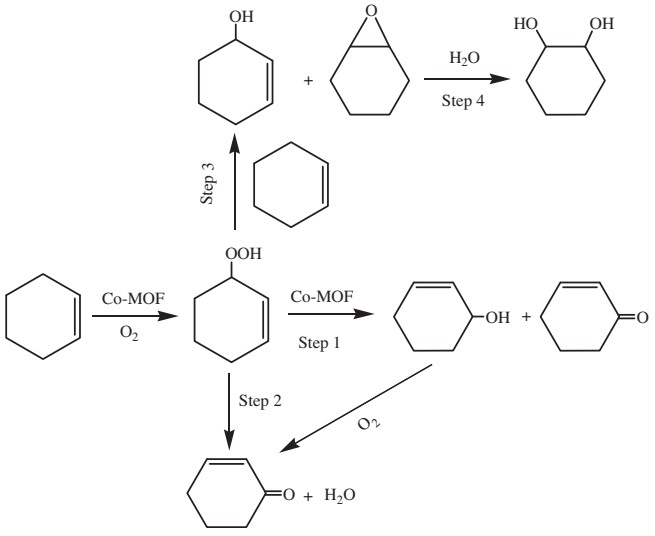

Scheme 2. Potential reaction pathways in the catalytic oxidation of cyclohexene with oxygen over $\{[Co_2(btec)(2,2'\text{-bipy})_2]\cdot H_2O\}_n$ (Co-MOF) catalyst.

cyclohexene with oxygen over $\{[Co_2(btec)(2,2'\text{-bipy})_2]\cdot H_2O\}_n$ were presumed in Scheme 2 according to the literature [3,7,9,25]. It is a complex radical-chain reaction and cyclohexenyl peroxyl radical (Cy-OO**.**) is the main chain propagator because the intermediate product of Cy-HP was detected in the reactions. Cy-HP was initially formed as the key primary product, which was prone to directly decompose to Cy-ol and Cy-one or to Cy-one and water in the presence of $\{[Co_2(btec)(2,2'\text{-bipy})_2]\cdot H_2O\}_n$ catalyst cycling between the $Co_{(II)}$ and $Co_{(III)}$ oxidation states (step 1 and 2). These reaction pathways provide the principal source of main products. Cy-HP can also change to Cy-ol and cyclohexene oxide through the epoxidation of cyclohexene, and cyclohexene oxide can react with water to produce 1,2-cyclohexanediol (step 3 and 4). When Cy-ol, Cy-one, cyclohexene oxide and 1,2-cyclohexanediol were obtained, a small fraction of them could be oxidized into deep oxygenated products. These reaction pathways were the source of by-products.

Side products such as cyclohexene oxide, 1,2-cyclohexanediol, hexanediol, adipic acid, and cyclohexanone were identified by comparison with standard samples (retention time in GC) and by-products were detected by GC–MS.

The effect of ligands on catalyst activity was examined for the oxidation of cyclohexene with oxygen in solvent-free conditions, and the results are listed in Table 2. For the blank test without the catalyst samples, small amounts of products were detected and the conversion was 2.7% (Entry 1). The conversion was only 12.3% with the Co-MOF-A catalyst, but using the Co-MOF-B catalyst yielded a superior conversion of 30.6% under the same reaction conditions (Entries 2 and 3). The Co-MOF-B catalyst exhibited an excellent catalytic activity and the decomposition of Cy-HP was accelerated, leading to the decrease of its selectivity. The difference between Co-MOF-A and Co-MOF-B was that Co-MOF-A was mixed with some residual H_4btec. A series of experiments were designed to obtain more information regarding the effects of ligands on the catalytic activity in the oxidation of cyclohexene. $Co(NO_3)_2\cdot 6H_2O$ was used as the catalyst with a conversion of 37.4% (Entry 4). The homogeneous Co^{2+} ions presented slightly improved catalytic activity than Co-MOF-B did. When using $Co(NO_3)_2\cdot 6H_2O$, the conversion decreased to 7.9% and 2.4% after the addition of H_4btec and 2,2′-bipy, respectively, and decreased to 2.1% when H_4btec and 2,2′-bipy were simultaneously added (Entries 5–7). These results indicated that H_4btec and 2,2′-bipy inhibited the catalytic activity of $Co(NO_3)_2\cdot 6H_2O$ in the oxidation of cyclohexene and that 2,2′-bipy has a stronger influence than H_4btec. Although H_4btec and 2,2′-bipy exert the same inhibitive effects, the products distributions vary greatly, which implied that the acting mechanisms of the two ligands might be different. In addition to H_4btec, other aromatic carboxylic acids were also analyzed. Remarkably, the conversion decreased to 8.1% and 8.3% after the addition of 1,2-benzenedicarboxylic acid and 1,3,5-benzenetricarboxylic acid, respectively, but increased to 42.6% and 48.7% after addition of benzoic acid and 1,4-benzenedicarboxylic acid, respectively (Entries 8–11). When 2,2′-bipy was subsequently added, the

Table 2
Effect of ligands on catalytic performance in cyclohexene oxidation.

Entry	Catalysts	Ligands	Conversion (%)	Selectivity (%)			
				Cy-ol	Cy-one	Cy-HP	Others
1[a]	–	–	2.7	8.5	21.8	68.0	1.7
2[a]	Co-MOF-A	–	12.3	8.1	22.3	64.9	4.7
3[a]	Co-MOF-B	–	30.6	9.8	26.8	48.4	15.0
4[b]	$Co(NO_3)_2{\cdot}6H_2O$	–	37.4	42.2	38.3	1.4	18.1
5[b]	$Co(NO_3)_2{\cdot}6H_2O$	H_4btec	7.9	17.7	29.7	47.2	5.4
6[b]	$Co(NO_3)_2{\cdot}6H_2O$	2,2′-bipy	2.4	26.9	47.3	19.1	6.7
7[b]	$Co(NO_3)_2{\cdot}6H_2O$	H_4btec and 2,2′-bipy	2.1	22.5	57.6	12.5	7.4
8[b]	$Co(NO_3)_2{\cdot}6H_2O$	1,2-benzenedicarboxylic acid	8.1	11.2	26.5	57.6	4.7
9[b]	$Co(NO_3)_2{\cdot}6H_2O$	1,3,5-benzenetricarboxylic acid	8.3	18.2	42.3	37.6	1.9
10[b]	$Co(NO_3)_2{\cdot}6H_2O$	benzoic acid	42.6	26.5	43.3	14.8	15.4
11[b]	$Co(NO_3)_2{\cdot}6H_2O$	1,4-benzenedicarboxylic acid	48.7	16.7	41.6	25.0	16.7
12[b]	$Co(NO_3)_2{\cdot}6H_2O$	benzoic acid and 2,2′-bipy	39.9	25.5	42.1	14.9	17.5
13[b]	$Co(NO_3)_2{\cdot}6H_2O$	1,4-benzenedicarboxylic acid and 2,2′-bipy	2.8	26.9	49.5	18.1	5.5
14[c]	$Co(NO_3)_2{\cdot}6H_2O$	–	21.8	11.7	33.7	47.3	7.3

[a] Reaction conditions: cyclohexene 5 mL, molar ratio of Co and cyclohexene 1:250, oxygen 2 MPa, temperature 343 K, time 6 h.
[b] Reaction conditions: cyclohexene 5 mL, molar ratio of Co and cyclohexene 1:125, molar ratio of Co and ligands 1:1, oxygen 2 MPa, temperature 343 K, time 6 h.
[c] Reaction conditions: cyclohexene 5 mL, Co^{2+} content in solution 24.7 mg/L, oxygen 2 MPa, temperature 343 K, time 6 h.

conversion changed slightly for benzoic acid, but decreased to 2.8% for 1,4-benzenedicarboxylic acid (Entries 12 and 13). These results suggested that for aromatic carboxylic acids containing two or more carboxyl groups, when two carboxyl groups are in ortho- and meta-positions, the ligand exerted a marked inhibitive effect; using 2,2′-bipy, also exerted the same inhibitive effect, but the influence can be eliminated by adding benzoic acid. To explain this complicated phenomenon, H_4btec was further studied. After the catalytic oxidation of cyclohexene, conducting ICP-OES analysis revealed that the concentration of the Co^{2+} ion in the filtered product solution was 136.3 mg/L by using $Co(NO_3)_2{\cdot}6H_2O$ (Entry 4) and 24.7 mg/L by using $Co(NO_3)_2{\cdot}6H_2O$ and H_4btec (Entry 5) (photographs of the products are displayed in Fig. S2). The Co^{2+} ion concentration in the solution decreased significantly after addition of H_4btec, which demonstrated that the inhibitive effect of H_4btec on $Co(NO_3)_2{\cdot}6H_2O$ was primarily caused by the immobilization and encapsulation of homogeneous Co^{2+} for the formation of a chelating structure. Subsequently, $Co(NO_3)_2{\cdot}6H_2O$ was used alone with the same residual Co^{2+} content (24.7 mg/L) in the aforementioned solutions, and the conversion was 21.8% (Entry 14), which is higher than 7.9% (Entry 5), which indicated that the residual Co^{2+} content in solutions essentially plays a role in the catalytic reactions; however, catalytic behavior was also hindered by H_4btec through another mechanism.

To obtain more information regarding the inhibitive mechanism of H_4btec, other heterogeneous catalysts were investigated in cyclohexene oxidation by excluding the possibility of physical adsorption and H_4btec residue, and the results are summarized in Table 3. A $\{[Co(2,2'\text{-dpa})(2,2'\text{-bipy})_2]{\cdot}2H_2O\}_n$ (2,2′-dpa: 2,2′-diphenic acid; 2,2′-bipy: 2,2′-bipyridine) metal–organic framework was prepared under hydrothermal conditions and a Cu-ELD/Co was prepared using copper electroless deposition as nanoparticles adsorbed on Co metal powders. For $\{[Co(2,2'\text{-dpa})(2,2'\text{-bipy})_2]{\cdot}2H_2O\}_n$ the conversion was 39.0%, and it decreased to 21.1% and 19.1% after addition of 0.5 and 1.0 mg H_4btec, respectively, and it decreased slightly when the amounts of H_4btec used increased (Entry 1–4). Similar changes in the conversions presented when combinations of the Cu-ELD/Co catalyst and H_4btec were used (Entry 6–9). These results indicated that when the amount of H_4btec used was equal in the cyclohexene oxidation using the two types of aforementioned heterogeneous catalysts, the conversion decrease was approximately equivalent regardless of the type and dosage of the catalysts. No interactions with H_4btec such as coordination, adsorption, and encapsulation were detected, particularly for the Cu-ELD/Co catalyst with a metal–metal alloy composition. Although H_4btec might interfere with the contact between the substrate and active sites of the catalyst, the conversions were not dramatically increased after the amount of catalysts used was doubled under the same reaction conditions (Entries 5 and 10). A conclusion is drawn that the inhibitive effect of H_4btec is independent of the heterogeneous catalysts but dependent on the cyclohexene oxidation process. Adding H_4btec presented low conversion with high Cy-HP selectivity, which suggests that the chemical changes involving Cy-HP were hindered by H_4btec and lead to the deceleration of the overall oxidation rate because of its aforementioned dominative role in cyclohexene oxidation. It

Table 3
Effect of H_4btec on catalytic performance in cyclohexene oxidation.

Entry	Catalysts	Catalyst amount (mg)	H_4btec amount (mg)	t (h)	Conversion (%)	Selectivity (%)			
						Cy-ol	Cy-one	Cy-HP	Others
1[a]	$\{[Co(2,2'\text{-dpa})(2,2'\text{-bipy})_2]{\cdot}2H_2O\}_n$	3.0	-	6	39.0	13.4	33.0	36.0	17.6
2[a]	$\{[Co(2,2'\text{-dpa})(2,2'\text{-bipy})_2]{\cdot}2H_2O\}_n$	3.0	0.5	6	21.1	9.7	26.2	53.0	11.1
3[a]	$\{[Co(2,2'\text{-dpa})(2,2'\text{-bipy})_2]{\cdot}2H_2O\}_n$	3.0	1.0	6	19.1	10.5	27.4	50.7	11.4
4[a]	$\{[Co(2,2'\text{-dpa})(2,2'\text{-bipy})_2]{\cdot}2H_2O\}_n$	3.0	10.0	6	14.1	6.9	19.7	63.7	9.7
5[a]	$\{[Co(2,2'\text{-dpa})(2,2'\text{-bipy})_2]{\cdot}2H_2O\}_n$	6.0	1.0	6	23.1	10.3	28.0	50.5	11.2
6[b]	Cu-ELD/Co	11.7	-	6	44.0	9.0	26.2	47.1	17.7
7[b]	Cu-ELD/Co	11.7	0.5	6	26.9	6.3	21.2	60.6	11.9
8[b]	Cu-ELD/Co	11.7	1.0	6	19.3	5.5	18.0	67.0	9.5
9[b]	Cu-ELD/Co	11.7	10.0	6	16.3	6.8	19.8	62.8	10.6
10[b]	Cu-ELD/Co	23.4	1.0	6	20.1	6.2	19.7	63.0	11.1

[a] Reaction conditions: cyclohexene 5 mL, oxygen 1.5 MPa, temperature 340 K.
[b] Reaction conditions: cyclohexene 5 mL, oxygen 2.0 MPa, temperature 349 K.

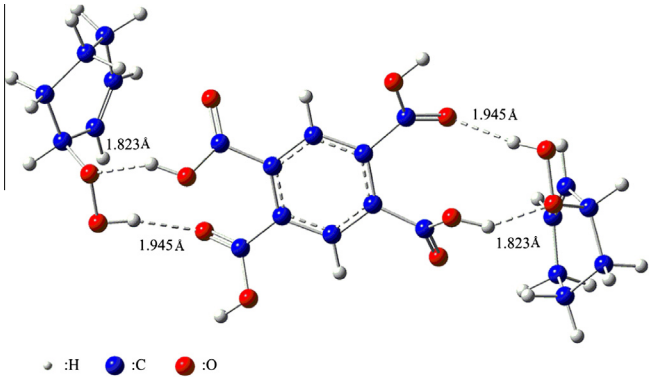

Fig. 6. Optimized geometries of the hydrogen bonds between Cy-HP and H_4btec.

is assumed that Cy-HP and H_4btec interact through a hydrogen-bonding network, and theoretical modeling and calculation were performed to preliminarily assume the reasonable configuration. The optimized geometries are illustrated in Fig. 6. The calculated results revealed that the oxygen atom connecting with cyclohexenyl in a Cy-HP –OOH group forms a hydrogen bond with the hydrogen atom in one H_4btec –COOH group and that the hydrogen atom in a Cy-HP –OOH group forms a hydrogen bond with carbonyl oxygen in another H_4btec –COOH group on one side. The length of the O–H···O hydrogen bond was 1.823 Å and 1.945 Å. A symmetrical construction was displayed on the other side of H_4btec. The hexatomic ring network built with the atoms to incorporate the two hydrogen bonds strengthened the stability of Cy-HP and the steric effect was also beneficial for protecting the Cy-HP –OOH group from catalyst attack.

(Fig. 7) shows the effects of reaction temperature on cyclohexene oxidation. When the temperature was increased from 323 to 343 K, the conversion of cyclohexene increased from 4.8% to 39.2%, but the total selectivity of Cy-ol, Cy-one and Cy-HP decreased from 98.2% to 82.1%, because of the formation of by products such as cyclohexene oxide, 1,2-cyclohexanediol, and hexanediol. The selectivity of Cy-HP decreased from 66.8% to 41.3%, whereas the selectivity of Cy-ol increased from 8.7% to 11%, and that of Cy-one increased from 22.7% to 29.8%, which indicated that Cy-HP rapidly decomposed into Cy-ol and Cy-one at high reaction temperatures. That the change in selectivity of Cy-HP was contrary to those of Cy-ol and Cy-one and that the selectivity of Cy-one was always higher than that of Cy-ol verified the aforementioned reaction pathways. The reaction temperature is one of the essential

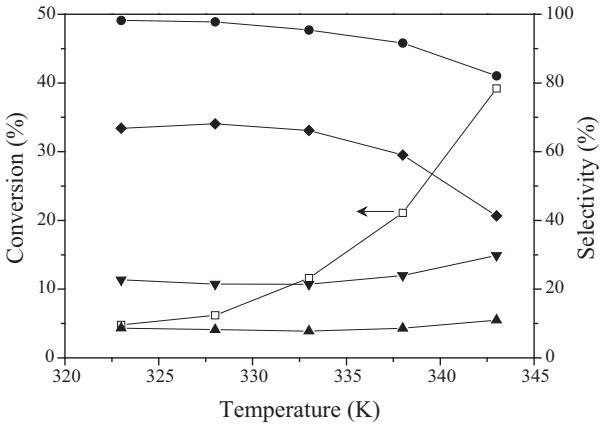

Fig. 7. Effect of reaction temperature on conversion and selectivity in cyclohexene oxidation. Reaction conditions: cyclohexene 5 mL, Co-MOF-B catalyst 57.3 mg, oxygen 2 MPa, time 6 h. □: Conversion of cyclohexene;▲: Selectivity of Cy-ol; ▼: Selectivity of Cy-one; ♦: Selectivity of Cy-HP; ●: Total selectivity of Cy-ol, Cy-one and Cy-HP.

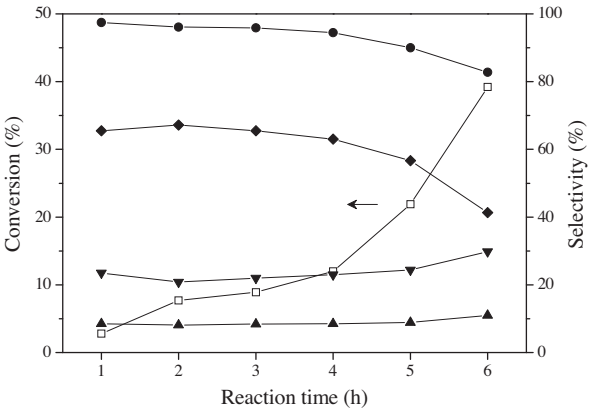

Fig. 8. Effect of reaction time on conversion and selectivity in cyclohexene oxidation. Reaction conditions: cyclohexene 5 mL, Co-MOF-B catalyst 57.3 mg, oxygen 2 MPa, temperature 343 K. □: Conversion of cyclohexene; ▲: Selectivity of Cy-ol; ▼: Selectivity of Cy-one; ♦: Selectivity of Cy-HP; ●: Total selectivity of Cy-ol, Cy-one and Cy-HP.

parameters in cyclohexene oxidations using the Co-MOF-B catalyst. The occurrence of deep oxidation leaded to carbonization at high temperatures, whereas no reaction occurred at low temperatures. Thus, the feasible reaction temperature is between 338 and 343 K.

(Fig. 8) illustrates the conversion and selectivity changes with different reaction times catalyzed using the Co-MOF-B catalyst at a temperature of 343 K. The conversion increased from 2.8% to 39.2% when the reaction time was extended from 1 h to 6 h. The selectivity of Cy-HP was 65.5% for 1 h, which suggested that Cy-HP was the primary product at the initial stage of reaction; however, it decreased to 41.3% when the reaction time was 6 h. Simultaneously, the selectivity of Cy-ol increased from 8.5% to 11% and the selectivity of Cy-one increased from 23.5% to 29.8%. The concentration of free radicals accumulated as the reaction time increased, which lead to the gradual increase of the reaction rate, the Cy-HP decomposition rate and the Cy-ol and Cy-one formation rate were simultaneously enhanced. The total selectivity of Cy-ol, Cy-one, and Cy-HP decreased linearly because peroxidation occurred as the reaction time increased. Therefore, in the following experiments, the oxidation was operated at 6 h in consideration of both the conversion and selectivity under the present reaction conditions.

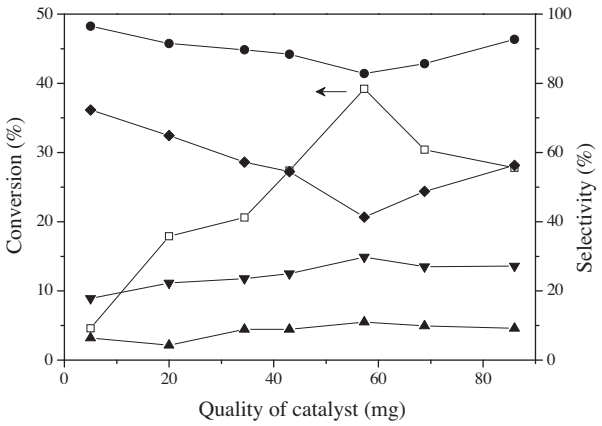

Fig. 9. Effect of Co-MOF-B catalyst amounts on conversion and selectivity in cyclohexene oxidation. Reaction conditions: cyclohexene 5 mL, oxygen 2 MPa, temperature 343 K, time 6 h. □: Conversion of cyclohexene; ▲: Selectivity of Cy-ol; ▼: Selectivity of Cy-one; ♦: Selectivity of Cy-HP; ●: Total selectivity of Cy-ol, Cy-one and Cy-HP.

(Fig. 9) depicts the effects of using different Co-MOF-B catalyst amounts on conversion and selectivity. The cyclohexene conversion increased as the amount of catalyst used increased. The conversion was 4.6% when 5.0 mg of catalyst was used and it reached a maximum value of 39.2% with 57.3 mg of catalyst. The conversion decreased by further increasing the amount of catalyst used, and it was 27.8% when the amount of catalyst used was 86.0 mg. The selectivity of Cy-HP presented a minimum value of 41.3% when 57.3 mg of catalyst was used, and the selectivity of Cy-ol and Cy-one simultaneously reached the maximum value. This indicates that the substrates adsorption in catalysts was balanced and that the catalytic activity was the most effective when 57.3 mg of catalyst was used. Enhancing the catalyst quality can inhibit reactions, which was identified as the so-called "catalyst inhibitor conversion" phenomenon already known for certain auto-oxidation processes [26]. A similar phenomenon has also been observed in previous studies [27,28]. Therefore, the optimal molar ratio of Co content and cyclohexne was 1:300.

Catalyst recycling is a crucial aspect of practical applications. The reusability of the Co-MOF-B catalyst in the oxidation of cyclohexene was examined under the conditions of 343 K and 2 MPa O_2. After a cyclohexene oxidation run, the solid catalyst was separated through centrifugation from the product solution and washed with ethanol several times, then dried at room temperature and reused for the next run under the same conditions. In the process of catalyst recycling, losing certain amounts of the catalyst is unavoidable. To maintain the same catalyst and substrate molar ratio, the amount of cyclohexene was decreased accordingly. As the results shown in Table 4, the conversion significantly decreased from 33.2% (the first run; Entry 1) to 19.7% (the second run; Entry 2), but did not considerably change in the subsequent runs (Entries 3–5). According to the ICP-OES analysis, the concentration of Co in the filtered product solution was 0.1385 mg/L after the first run and 0.024 mg/L after the fifth run, which means that approximately 0.89 and 0.32 wt.% of Co in the Co-MOF-B catalyst leached from the matrix, respectively. The leached Co amount was as minimal as the leached Au amount from Au/La-OMS-2 (0.24) catalyst in the solvent-free system [7]. To prove the heterogeneous nature of the catalytic reaction, the conventional filtration experiment was carried out over Co-MOF-B catalyst. As the results shown in Table 5 (Entries 1–5), when the solid catalyst was filtered off from the reaction mixture after reacting for 4 h, the conversion of cyclohexene in the filtrate increased from 12.0% to 13.8% in 1 h and to 16.3% in 2 h respectively, which indicated that the leached Co species were not responsible for the obtained catalytic activity over Co-MOF-B catalyst. So it is confirmed that the present reactions are truly performed over the Co-MOF-B catalyst surface heterogeneously. Therefore, it was suggested that the Co-MOF-B catalyst surface was surrounded by organic residue after the cyclohexene oxidation runs, as shown in Fig. 4, which affected the accessibility of reactant molecules to metal active sites and decreased the catalytic activity in the recycling tests. Because of this possibility, the catalyst was collected after a cyclohexene oxidation run, treated using $scCO_2$-expanded ethanol system, and reused in a second run. Remarkably, the conversion of cyclohexene was 53.6% (Entry 6) and the activity was higher than that of the fresh catalyst, which suggested that this method not only realized catalyst regeneration, but also increased the activity of catalyst. More details were obtained from the textural properties (Table 6). The BET surface areas and pore volumes of the Co-MOF-B samples were determined by analyzing the N_2 adsorption–desorption data. The Co-MOF-B samples exhibited low surface areas and small pore volumes, which can be attributed to the high crystallinity of the layer microstructure, which is consistent with the results of the TEM analysis (Fig. 5). The textural properties of the Co-MOF-B catalyst are similar to those of the Mg/Al reconstructed hydrotalcite layered crystals prepared by Pavel et al. [29,30]. Based on the results, it can be assumed that the accessibility of substrate and catalytic active

Table 4
Recycle and regeneration of Co-MOF-B catalyst in cyclohexene oxidation.

Entry	Run times	Conversion (%)	TOF (h^{-1})[b]	Selectivity (%)			
				Cy-ol	Cy-one	Cy-HP	Others
1	first	33.2	16.6	9.9	31.6	48.5	10.0
2	second	19.7	9.9	11.7	31.3	49.7	7.3
3	third	15.1	7.6	10.5	28.1	55.9	5.5
4	fourth	15.2	7.6	13.3	34.1	50.4	2.2
5	fifth	19.5	9.8	12.8	33.6	48.9	4.7
6[a]	second	53.6	26.8	13.0	38.6	28.8	19.6

Reaction conditions: cyclohexene 5 mL, molar ratio of Co and cyclohexene 1:300, oxygen 2 MPa, temperature 343 K, time 6 h.
[a] The catalyst was collected after one cyclohexene oxidation run and treated with a $scCO_2$-expanded ethanol system.
[b] Turnover Frequency (TOF) is calculated by expression of (moles of cyclohexene consumed)/[(mole of total Co^{2+} ions in catalyst samples used) × time (h)].

Table 5
Catalytic oxidation of cyclohexene with oxygen in different reaction conditions.

Entry	Catalyst	Time (h)	Conversion (%)	TOF (h^{-1})	Selectivity (%)			
					Cy-ol	Cy-one	Cy-HP	Others
1[a]	$\{[Co_2(btec)(2,2'\text{-bipy})_2]\cdot H_2O\}_n$	4	12.0	6.0	8.5	23.0	63.0	5.5
2[a]	$\{[Co_2(btec)(2,2'\text{-bipy})_2]\cdot H_2O\}_n$	5	21.9	11.0	8.9	24.4	56.7	10.0
3[a]	$\{[Co_2(btec)(2,2'\text{-bipy})_2]\cdot H_2O\}_n$	6	39.2	19.6	11.0	29.8	41.3	17.9
4[a,b]	–	5	13.8	6.9	8.0	28.4	53.0	10.6
5[a,c]	–	6	16.3	8.2	7.3	28.4	56.8	7.5
6[d] [3]	$[Co_2(DOBDC)(H_2O)_2]\cdot 8H_2O$	20	32.8	8.0	39.3	51.2	–	–
7[e] [7]	Au/La-OMS-2	24	48.0	–	40.3	44.0	–	–
8[f] [8]	Cr-MCM-41	24	52.2	–	11.2	71.2	14.2	–

[a] Reaction conditions: cyclohexene 5 mL, molar ratio of Co and cyclohexene 1:300, oxygen 2 MPa, temperature 343 K.
[b] The catalyst was filtered off from the reaction mixture after reacting for 4 h and then kept reacting for 1 h.
[c] The catalyst was filtered off from the reaction mixture after reacting for 4 h and then kept reacting for 2 h.
[d] Reaction conditions: catalyst 50 mg, cyclohexene 5 mL, temperature 353 K, oxygen balloon.
[e] Reaction conditions: catalyst 0.2 g, cyclohexene 20 mL, temperature 353 K, oxygen 0.4 MPa.
[f] Reaction conditions: catalyst 20 mg, cyclohexene 1 g, temperature 343 K, oxygen 1 atm.

Table 6
Textural properties of Co-MOF-B samples.

Samples	BET surface area ($m^2\ g^{-1}$)	Pore Volume ($cm^3\ g^{-1}$)
Fresh Co-MOF-B	1.6	0.0084
Co-MOF-B[a]	2.0	0.0126
Co-MOF-B[b]	3.1	0.0151

[a] The catalyst sample was collected after one cyclohexene oxidation run.
[b] The catalyst sample was collected after one cyclohexene oxidation run and treated with a $scCO_2$-expanded ethanol system.

sites mainly occurred on the catalyst surface because of the poor porous structure. Therefore, the regeneration and active enhancement of catalysts by treating with $scCO_2$-expanded ethanol were attributed to these aspects: first, the surface area of the Co-MOF-B catalyst samples increased because the crystal particles were crushed in the treatment process, and the crystal particle size is an essential factor affecting the catalytic activity; second, the organic residue on the surface of catalyst samples after a reaction was extracted using $scCO_2$-expanded ethanol; using $scCO_2$-expanded liquid aids separation because it possesses unique properties, such as low viscosity, high diffusivity, near-zero surface tension, and high solubility for a wide range of organic compounds [31], and also excess CO_2 weakens the interactions between certain polymers and matrices [32]. The regeneration of a deactivated catalyst through supercritical CO_2 extraction has also been reported in the literature [33,34]. Furthermore, the TOF values of the Co-MOF-B catalyst were relatively low, which was calculated according to the mole of total Co^{2+} ions in the catalyst samples used. It was revealed that only the Co sites at the outer surface of catalysts are accessible and involved in the catalytic reactions, so the real TOF values must be higher than the calculated TOF values evidently. Finally, in comparison with the activities of heterogeneous catalysts such as $[Co_2(DOBDC)(H_2O)_2]\cdot 8H_2O$ Co-MOF (DOBDC = 2,5-dihydroxyterephthalic acid), Au/La-OMS-2, and Cr-MCM-41 in the similar reaction conditions reported in the literature (Table 5 Entries 6–8), comparable reaction conversion and TOF value were obtained with the present $\{[Co_2(btec)(2,2'\text{-bipy})_2]\cdot H_2O\}_n$ Co-MOF catalyst.

4. Conclusions

In summary, the Co (II) metal–organic framework $\{[Co_2(btec)(2,2'\text{-bipy})_2]\cdot H_2O\}_n$ exhibited effective performance in the allylic oxidation of cyclohexene with oxygen under solvent-free conditions. It exhibited high crystallinity with a compact layered microstructure and poor porous texture, which was determined by the coordination modes and crystal growth characteristics. It behaved as a heterogeneous catalyst, which was deactivated in catalyst recycling because the formation of organic residue adsorbed on the surface covered the active Co^{2+} sites. Catalyst regeneration was achieved and the catalytic activity was enhanced by treating with a $scCO_2$-expanded ethanol system, which was attributed to extracting organic residue and crushing crystal particles. The inhibitive effects of H_4btec and other ligands on cyclohexene oxidation was detected, regarding aromatic carboxylic acids containing two or more carboxyl groups, when two carboxyl groups were in ortho- and meta-positions, the ligand exerted a marked inhibitive effect. The research results confirmed that the inhibitive effect of H_4btec is independent of the heterogeneous catalyst but dependent on cyclohexene oxidation reactions, which is explained by the presumed hydrogen bonds between H_4btec and the 2-cyclohexene-1-hydroperoxide intermediate.

Acknowledgments

The authors gratefully acknowledge the financial support from the Natural Science Foundation of China (NSFC 21163011), the Natural Science Foundation of Inner Mongolia (2013MS0208), and the Science Research Projects of Inner Mongolia University (NJ10072).

Appendix A. Supplementary material

Supplementary data associated with this article can be found, in the online version, at http://dx.doi.org/10.1016/j.ica.2014.06.005. These data include MOL files and InChiKeys of the most important compounds described in this article.

References

[1] R.A. Sheldon, J.K. Kochi, Metal Catalyzed Oxidations of Organic Compounds, Academic Press, New York, 1981.
[2] K.C. Gupta, A.K. Sutar, C. Lin, Coord. Chem. Rev. 253 (2009) 1926.
[3] Y. Fu, D. Sun, M. Qin, R. Huang, Z. Li, RSC Adv. 2 (2012) 3309.
[4] S.H. Jhung, J. Lee, A.K. Cheetham, G. Férey, J. Chang, J. Catal. 239 (2006) 97.
[5] M. Ghiaci, B. Aghabarari, A.M. Botellho do Rego, A.M. Ferraria, S. Habibollahi, Appl. Catal. A: Gen. 393 (2011) 225.
[6] H. Huang, H. Zhang, Z. Ma, Y. Liu, H. Ming, H. Li, Z. Kang, Nanoscale 4 (2012) 4964.
[7] Z. Cai, M. Zhu, J. Chen, Y. Shen, J. Zhao, Y. Tang, X. Chen, Catal. Commun. 12 (2010) 197.
[8] S.E. Dapurkar, H. Kawanami, K. Komura, T. Yokayama, Y. Ikushima, Appl. Catal. A: Gen. 346 (2008) 112.
[9] J. Tong, Y. Zhang, Z. Li, C. Xia, J. Mol. Catal. A: Chem. 249 (2006) 47.
[10] B. Ye, M. Tong, X. Chen, Coord. Chem. Rev. 249 (2005) 545.
[11] M. Tonigold, Y. Lu, B. Bredenkötter, B. Rieger, S. Bahnmüller, J. Hitzbleck, G. Langstein, D. Volkmer, Angew. Chem., Int. Ed. 48 (2009) 7546.
[12] E.Q. Procopio, F. Linares, C. Montoro, V. Colombo, A. Maspero, E. Barea, Jorge A.R. Navarro, Angew. Chem., Int. Ed. 49 (2010) 7308.
[13] M. Tonigold, Y. Lu, A. Mavrandonakis, A. Puls, R. Staudt, J. Möllmer, J. Sauer, D. Volkmer, Chem. Eur. J. 17 (2011) 8671.
[14] Z. Lin, M. Tong, Coord. Chem. Rev. 255 (2011) 421.
[15] H. Wu, H. Liu, J. Wang, B. Liu, J. Ma, Y. Liu, Y. Liu, Cryst. Growth Des. 11 (2011) 2317.
[16] O. Fabelo, J. Pasán, L. Cañadillas-Delgado, F.S. Delgado, A. Labrador, F. Lloret, M. Julve, C. Ruiz-Pérez, Cryst. Growth Des. 8 (2008) 3984.
[17] Z. Su, M. Chen, T. Okamura, M. Chen, S. Chen, W. Sun, Inorg. Chem. 50 (2011) 985.
[18] K. Brown, S. Zolezzi, P. Aguirre, D. Venegas-Yazigi, V. Paredes-García, R. Baggio, M.A. Novak, E. Spodine, Dalton Trans. (2009) 1422.
[19] D. Jiang, T. Mallat, D.M. Meier, A. Urakawa, A. Baiker, J. Catal. 270 (2010) 26.
[20] M. J. Plater, M. R. St J. Foreman, R. A. Howie, J. M. S. Skakle, A. M. Z. Slawin, Inorg. Chim. Acta, 315 (2001) 126.
[21] Y. Li, H. Zhang, E. Wang, N. Hao, C. Hu, Y. Yan, D. Hall, New J. Chem. 26 (2002) 1619.
[22] Y. Qi, H. Li, F. Guo, M. Cao, C. Hu, J. Coord. Chem. 59 (2006) 505.
[23] G.M. Sheldrick, SHELXS97,Program for Crystal Structure Solution, University of Göttingen, Germany, 1997.
[24] G.M. Sheldrick, SHELXL97, Program for Crystal Structure Refinement, University of Göttingen, Germany, 1997.
[25] H. Weiner, A. Trovarelli, R.G. Finke, J. Mol. Catal. A: Chem. 191 (2003) 217.
[26] J.F. Black, J. Am. Chem. Soc. 100 (1978) 1311.
[27] C. Guo, Q. Liu, X. Wang, H. Hu, Appl. Catal. A: Gen. 282 (2005) 55.
[28] G. Huang, Y. Guo, H. Zhou, S. Zhao, S. Liu, A. Wang, J. Wei, J. Mol. Catal. A: Chem. 273 (2007) 144.
[29] O.D. Pavel, R. Bîrjega, M. Che, G. Costentin, E. Angelescu, S. Şerban, Catal. Commun. 9 (2008) 1974.
[30] E. Angelescu, R. Ionescu, O.D. Pavel, R. Zăvoianu, R. Bîrjega, C.R. Luculescu, M. Florea, R. Olar, J. Mol. Catal. A: Chem. 315 (2010) 178.
[31] G.R. Akien, M. Poliakoff, Green Chem. 11 (2009) 1083.
[32] R. Liu, C. Wu, Q. Wang, J. Ming, Y. Hao, Y. Yu, F. Zhao, Green Chem. 11 (2009) 979.
[33] L. Vradman, M. Herskowitz, E. Korin, J. Wisniak, Ind. Eng. Chem. Res. 40 (2001) 1589.
[34] E.S. Lokteva, A.E. Lazhko, E.V. Golubina, V.V. Timofeev, A.V. Naumkin, T.V. Yagodovskaya, S.N. Gaidamaka, V.V. Lunin, J. Supercrit. Fluids 58 (2011) 263.